Article | Received 29 June 2026; Revised 2 September 2026; Accepted 3 November 2026; Published 27 November 2026
https://doi.org/10.55092/acr20260016

Aspartame promotes tumor growth through stress-induced metabolic reprogramming

Miki Sato[1,2,3,†], Honoka Imagawa[1,4,†], Ayana Sakamoto[1,5,†], Alice Ferrari[1,6,†], Bo Xu[1,7], Chisato Iwabuchi-Yoshida[1], Cayla Boycott[1], Ritsuko Ando[1], Yoshitaka Yamazaki[1,8], Rika Tsuchida[1], Kazuyuki Yamagata[1,4] and Tsuyoshi Osawa[1,4,9,10,*]

[1] Division of Nutriomics and Oncology, RCAST, The University of Tokyo, Tokyo, Japan
[2] Shibuya Senior High School, Tokyo, Japan
[3] UTokyoGSC-Next, JST STELLA Program, Tokyo, Japan
[4] Department of Chemistry and Biotechnology, Graduate School of Engineering, the University of Tokyo, Tokyo, Japan
[5] Department of Chemistry, Carleton College, Northfield, USA
[6] Department of Biological Sciences, University of Milano, Bicocca, Italy
[7] Department of Pathology and Forensic Medicine, School of Basic Medical Sciences, Zhengzhou University, Zhengzhou, China
[8] Department of Physiology, Showa Medical University Graduate School of Pharmacy, Tokyo, Japan
[9] Department of Biological Sciences, Graduate School of Science, The University of Tokyo, Tokyo, Japan
[10] Graduate School of Medicine and Dentistry, Institute of Science Tokyo, Tokyo, Japan

† These authors contributed equally to this work.

* Correspondence author; E-mail: osawa@lsbm.org.

Highlights:

- Aspartame has limited cytotoxic effects on cancer cells.
- RNA sequencing (RNA-seq) reveals activation of xenobiotic metabolism by aspartame.
- Aspartame induces stress-associated metabolic remodeling.
- High-concentration aspartame exposure is associated with enhanced tumor growth.

Abstract: Aspartame is among the most widely consumed artificial sweeteners, yet how it influences cancer remains poorly understood, because most prior work has addressed cancer incidence and carcinogenicity rather than the cellular and metabolic responses it elicits. Here, we integrated transcriptomic and metabolomic approaches to characterize the effects of aspartame on human cancer cells and on tumor growth *in vivo*. In multiple cancer cell lines, aspartame had only modest effects on short-term proliferation and did not induce substantial apoptotic or necroptotic cell death. Ribonucleic acid (RNA) sequencing of HCT116 and HepG2 cells instead revealed a conserved transcriptional response, characterized by activation of xenobiotic metabolism and suppression of metallothionein-dependent metal homeostasis,

Copyright © 2026 by the authors. Published by ELSP. This work is licensed under Creative Commons Attribution 4.0 International License, which permits unrestricted use, distribution, and reproduction in any medium provided the original work is properly cited.

which we confirmed by quantitative polymerase chain reaction (PCR). Metabolomic profiling demonstrated metabolic remodeling involving pathways associated with glycolysis, the pentose phosphate pathway, and the Warburg effect, accompanied by suppression of pathways for cell cycle progression, deoxyribonucleic acid (DNA) repair, and ribosome biogenesis. In a colorectal cancer xenograft model, continuous oral aspartame intake significantly accelerated HCT116 tumor growth without changes in body weight, serum liver enzymes, triglycerides, or cholesterol. Metabolomic analysis of excised tumors confirmed enhanced central carbon metabolism, including elevated acetyl-coenzyme A (acetyl-CoA), citrate, and coenzyme A, together with decreased amino acids linked to transfer RNA (tRNA) charging. Collectively, these findings indicate that aspartame induces stress-associated metabolic remodeling and is associated with enhanced tumor growth under high-exposure conditions rather than direct cytotoxicity, providing mechanistic insight into the metabolic consequences of aspartame exposure in cancer.

Keywords: aspartame; artificial sweetener; metabolic remodeling; stress response; xenobiotic metabolism; tumor growth; cancer

1. Introduction

Excessive dietary sugar intake has been associated with an increased risk of diabetes, cardiovascular disease, cancer, and neurological disorders [1–4]. Growing awareness of these risks has led to a demand for low-calorie alternatives to sugar. Thus, non-nutritive sweeteners (NNS) were developed and subsequently integrated into a wide range of food and beverage products [5–7]. Aspartame is a widely used artificial sweetener due to its near-zero caloric value while retaining an intense sweetness that is approximately 200 times greater than that of sucrose [5,7,8]. Aspartame is a dipeptide composed of the amino acids: phenylalanine and aspartic acid. Upon digestion, aspartame is hydrolyzed into the metabolites: phenylalanine (50%), aspartic acid (40%), and methanol (10%) [5,9]. The U.S. Food and Drug Administration (FDA) deems aspartame consumption to be safe within the recommended daily intake limit of 50 mg per kilogram of body weight [5,7]. However, there is controversy regarding the health risks of long-term aspartame consumption, especially due to inconsistencies in the results of different studies regarding the link between cancer and aspartame [5,6]. This controversy was brought into sharp focus in 2023, when the International Agency for Research on Cancer (IARC) classified aspartame as “possibly carcinogenic to humans” (Group 2B) on the basis of limited evidence for hepatocellular carcinoma, whereas the Joint Food and Agriculture Organization (FAO)/World Health Organization (WHO) Expert Committee on Food Additives (JECFA) concurrently reaffirmed the acceptable daily intake and found no convincing evidence of adverse effects [10,11]. Both bodies, however, explicitly called for further mechanistic investigation, underscoring the need to clarify how aspartame might influence cancer cells at the molecular level [11,12].

Numerous studies have investigated the connection between artificial sweetener consumption and cancer risk, and through an epidemiological lens former studies have demonstrated a potential risk of cancer associated with aspartame consumption [6]. However, a comprehensive metabolomic analysis aimed at understanding the mechanisms underlying cancer development and progression has not yet been performed. Although epidemiological and toxicological studies have provided important insights into the potential health effects of aspartame, the biological mechanisms underlying its influence on tumor development remain poorly understood, as most previous studies have focused on cancer

incidence or carcinogenicity, whereas relatively little attention has been paid to the cellular and metabolic responses induced by aspartame exposure. Because metabolic reprogramming is a hallmark of cancer progression and plays a critical role in supporting tumor growth [13–15], investigating the metabolic consequences of aspartame exposure may provide important clues regarding its potential effects on cancer biology.

Recent advances in transcriptomic and metabolomic technologies have enabled comprehensive characterization of cellular responses to environmental and dietary factors, and integrated analyses of gene expression and metabolism can reveal pathways that are altered before overt phenotypic changes become apparent, thereby helping to identify mechanisms through which dietary compounds influence tumor behavior [15,16]. In the present study, we therefore investigated the effects of aspartame on cancer cells using transcriptomic and metabolomic approaches. We first examined the impact of aspartame on cell growth and cell death in multiple human cancer cell lines, then performed ribonucleic acid sequencing (RNA-seq) and untargeted metabolomic analyses to identify molecular pathways altered by aspartame exposure, and finally evaluated the effects of aspartame on tumor growth and tumor metabolism in a colorectal cancer xenograft model. Our findings demonstrate that aspartame induces extensive metabolic reprogramming characterized by alterations in central carbon metabolism and is associated with enhanced tumor growth *in vivo*.

2. Methods

(1) Cell culture

Human colorectal cancer (HCT116) and human hepatocellular carcinoma (HepG2) cells, were sourced from the American Type Culture Collection (ATCC, Manassas, VA, USA). Cells were cultivated in Dulbecco's modified Eagle's medium (DMEM) (Nacalai Tesque, Kyoto, Japan) with 10% fetal bovine serum (FBS) (Nichirei) under standard conditions (37 °C, 5% CO_2). All human cell lines were authenticated by short tandem repeat (STR) profiling by the supplier (ATCC). Cell lines were routinely tested for mycoplasma contamination using polymerase chain reaction (PCR)-based detection methods and were confirmed to be negative.

(2) Aspartame preparation and treatment

For *in vitro* treatments, aspartame (FUJIFILM Wako) was dissolved in DMEM, vortexed, and sonicated in a bath sonicator for 2–3 min, then further diluted in DMEM to the final concentrations indicated. For the pH- and osmolality-adjusted control experiments, the pH of the 30 mM aspartame medium was measured, and control medium was titrated to the same pH; osmolality was measured with a freezing-point osmometer and matched between conditions by addition of an inert osmolyte, so that cells were exposed to the same extracellular pH and osmolality as the 30 mM aspartame condition in the absence of aspartame. We note that dedicated methanol-only and reconstituted combined hydrolysis-product (phenylalanine + aspartic acid + methanol) controls were not performed in the present study.

(3) Cell proliferation assay

Cells were seeded in 96-well plates, cultured under indicated conditions, fixed with 10% trichloroacetic acid, and stained with 0.4% sulforhodamine B (SRB) in 1% acetic acid. After washing and solubilization

in 10 mM tris(hydroxymethyl)aminomethane (Tris) solution, absorbance was measured at 570 nm using an ARVO microplate reader (PerkinElmer).

(4) Immunoblot analysis

Cells were lysed in radioimmunoprecipitation assay (RIPA) buffer (Wako #182-02451) supplemented with protease (Roche #11697498001) and phosphatase inhibitors (Roche, #4906845001). Proteins were separated by sodium dodecyl sulfate–polyacrylamide gel electrophoresis (SDS-PAGE), transferred to nitrocellulose or polyvinylidene difluoride (PVDF) membranes, blocked, and probed with primary antibodies overnight at 4 °C. After incubation with horseradish peroxidase (HRP)-conjugated secondary antibodies, signals were detected using FUSION (Vilber). Antibodies: anti-glutathione peroxidase 4 (GPX4; Cell Signaling Technology [CST], #52455), anti-receptor-interacting protein kinase 1 (RIP; CST, #3493), anti-phospho-RIP (CST, #65746), anti-mixed lineage kinase domain-like protein (MLKL; CST, #14993), anti-phospho-MLKL (CST, #91689), anti-cleaved Caspase-3 (CST, #9661S), anti-Caspase-3 (CST, #9662S), β-actin (Sigma-Aldrich, #A5441).

(5) Real-time PCR

Total ribonucleic acid (RNA) was extracted from cells using ISOGEN reagent (Nippon Gene, Tokyo, Japan) according to the manufacturer's instructions. Complementary deoxyribonucleic acid (cDNA) was synthesized from total RNA using PrimeScript reverse transcriptase (Takara Bio, Shiga, Japan). Quantitative real-time PCR (qPCR) was performed using THUNDERBIRD SYBR qPCR Mix (Toyobo, Osaka, Japan) with gene-specific primers. The relative messenger RNA (mRNA) expression levels were normalized to actin beta (ACTB) as an internal control. Cycle threshold (Ct) values were used to calculate relative gene expression using the comparative Ct method, and fold changes were determined using the $2^{-\Delta\Delta CT}$ method.

The primer sequences were as follows: cytochrome P450 family 24 subfamily A member 1 (CYP24A1), forward 5′-GCCGTATTTAAAAGCCTGTCTGAA-3′ and reverse 5′-ACCTGGGTATTT AGCATGAGCACTG-3′; metallothionein 1F (MT1F), forward 5′-CTGCTTCTTCGCTTCTCTCTT-3′ and reverse 5′-TCTTGCAGGAGGTGCATTT-3′; ACTB, forward 5′-AGAAGGAGATCACTGCCCTGGCACC-3′ and reverse 5′-CCTGCTTGCTGATCCACATCTGCTG-3′.

(6) Alanine aminotransferase (ALT) Aspartate aminotransferase (AST) Cholesterol Triglycerides (TG) measurements

Immediately following mouse euthanasia, plasma was separated from whole blood by centrifugation in a 1.5 mL tube. AST and ALT were measured in mouse plasma using the LabAssay™ AST/ALT kits (Fuji Film, 299-97601/293-97501, respectively) per the manufacturer's instructions. TG, cholesterol were determined using the LabAssay™ Triglyceride/Cholesterol measurement kit (Fuji Film, 291-94501/ 293-93601, respectively) as per the manufacturer's instructions.

(7) Metabolome analysis

Cells were washed with 5% mannitol and extracted with methanol containing internal standards (methionine sulfone, camphorsulfonic acid, 2-(*N*-morpholino)ethanesulfonic acid (MES)). After chloroform-water extraction, the aqueous phase was ultrafiltrated and dried. Samples were analyzed by capillary electrophoresis–time-of-flight mass spectrometry (CE-TOF-MS) (Agilent Technologies). Metabolite concentrations were quantified using standard mixtures. For tumor-tissue analyses, snap-frozen

xenograft tumors were homogenized and extracted by the same procedure. Aspartame and its hydrolysis products (phenylalanine and aspartic acid) were identified on the basis of their migration time and accurate mass relative to authentic analytical standards analyzed under identical conditions, and were quantified against calibration curves prepared from these standards; values are expressed as nmol/g tissue.

(8) RNA-seq

Total RNA was extracted from tissue or cell lysates with the use of a PureLink RNA Mini Kit (Thermo Fisher Scientific), and the quality of the purified RNA was assessed with a 2100 Bioanalyzer (Agilent). After mRNA selection with the use of a NEBNext Poly(A) mRNA Magnetic Isolation Module (New England BioLabs), libraries were prepared with the use of a NEBNext Ultra Directional RNA Library Prep Kit for Illumina (New England BioLabs). The cDNAs were sequenced with a NovaSeq 6000 system.

(9) RNA-seq data analysis

Quality control of the 300-bp paired-end reads was performed using FastQC, and adapter and low-quality sequence trimming was conducted using Trimmomatic. Reads were aligned to the human reference genome (hg38) using Hierarchical Indexing for Spliced Alignment of Transcripts 2 (HISAT2), and gene-level read counts were obtained using featureCounts. Differential expression analysis was performed using the Tag Count Comparison (TCC) package in R/Bioconductor, and differentially expressed genes (DEGs) were defined as those with false discovery rate (FDR) < 0.05 and absolute log2 fold change (|log2FC|) > 1. Expression levels were additionally normalized as transcripts per million (TPM). Volcano plots were generated using the EnhancedVolcano package in R. Genes meeting the DEG criteria were subjected to pathway enrichment analysis using Integrated Molecular Pathway-Level Analysis (IMPaLA; version 13). Gene Set Enrichment Analysis (GSEA) was performed using the Hallmark gene set collection from Molecular Signatures Database (MSigDB). Heatmaps and hierarchical clustering were generated using the gplots package in R. RNA from three independent biological replicates per group was analyzed.

(10) Xenograft experiments

Female C.B-17/IcrHsd-Prkdc scid mice aged 7 weeks were purchased from SLC Japan, Inc. The animals were housed in individual cages in a temperature- and light-controlled environment and had *ad libitum* access to chow and water. All mouse experiments were approved by the University of Tokyo Animal Care and Use Committee. Only female mice were used in this study. Therefore, potential sex-based differences were not evaluated and represent a limitation of this study.

Seven-week-old C.B-17/IcrHsd-Prkdc scid female mice were subcutaneously injected with 1×10^7 HCT116 cells in 100 µL phosphate-buffered saline (PBS). From the day 6 after tumor implantation, mice were provided with either drinking water containing aspartame or regular drinking water ad libitum throughout the experimental period. Tumor volumes were measured three times weekly and calculated as (length × width^2)/2. Mice were randomly allocated to the control and aspartame groups after tumor cell implantation, and tumor-volume measurements and downstream omics analyses were performed without reference to group allocation. No formal a priori sample-size calculation was performed; the group size (n = 5 mice per group) was based on standard practice for subcutaneous xenograft studies, and the limited sample size is acknowledged as a study limitation. All five tumors per group were included in the *in vivo* metabolomic analysis.

To estimate actual aspartame exposure, daily water consumption was measured under the same housing and treatment conditions used in the xenograft study. The average water intake was approximately 3.5 mL per mouse per day, corresponding to an estimated aspartame intake of 30.9 mg/day (approximately 1545 mg/kg/day). The corresponding human equivalent dose was estimated to be approximately 125 mg/kg/day.

(11) Statistical analysis

Data are presented as mean ± standard error of the mean (SEM) unless otherwise indicated. Statistical analyses were performed using GraphPad Prism 10. Comparisons between two groups were performed using Student's t-test. Multiple-group comparisons were performed using one-way analysis of variance (ANOVA) followed by Tukey's multiple-comparison test. Tumor growth curves, which comprise repeated tumor-volume measurements from the same animals over time, were analyzed using a repeated-measures (mixed-effects) model with treatment and time as factors, followed by Tukey's multiple-comparison test. $P < 0.05$ was considered statistically significant. Statistical significance is indicated as *$P < 0.05$, **$P < 0.01$, ***$P < 0.005$, and ****$P < 0.001$.

3. Results

3.1. Aspartame modestly affects cancer cell growth without inducing apoptotic or necroptotic cell death

To evaluate the effect of aspartame on cancer cell proliferation, multiple human cancer cell lines were treated with aspartame at concentrations of 0.3, 3, and 30 mM for 24 h (Figure 1a), followed by SRB assay analysis [17]. Aspartame treatment produced only modest effects on cell growth in most cell lines, although growth inhibition was observed at 30 mM in several cell lines (Figure 1b). Because aspartame is metabolized into aspartic acid, phenylalanine, and methanol (Figure 1c), we next examined whether the observed effects could be explained by its degradation products. Cells were treated with equivalent concentrations of aspartic acid or phenylalanine and analyzed by SRB assay. Compared with aspartame, both aspartic acid and phenylalanine induced stronger growth suppression at 30 mM in several cell lines (Figure 1b), suggesting that the cellular effects of aspartame cannot be fully attributed to its constituent amino acids. During culture, we noticed a marked color change in the medium containing 30 mM aspartame, and measurement of medium pH revealed a significant decrease only in the 30 mM treatment group (Figure 1d), indicating that part of the growth inhibition observed at this concentration may be associated with medium acidification.

To further characterize the cellular response, floating and attached HCT116 cells were quantified after 72 h of aspartame treatment. The proportion of floating cells was highest in the 30 mM treatment group, consistent with the medium acidification observed only at this concentration (Figure 1e). However, immunoblot analysis showed no evident activation of apoptotic markers, including cleaved caspase-3, following 24 h of aspartame treatment (Figure 1f). In addition, markers of necroptosis, including phosphorylated RIP (p-RIP) and phosphorylated MLKL (p-MLKL), were not increased by aspartame treatment [18]. These results suggest that aspartame does not induce substantial apoptotic or necroptotic cell death under the conditions tested.

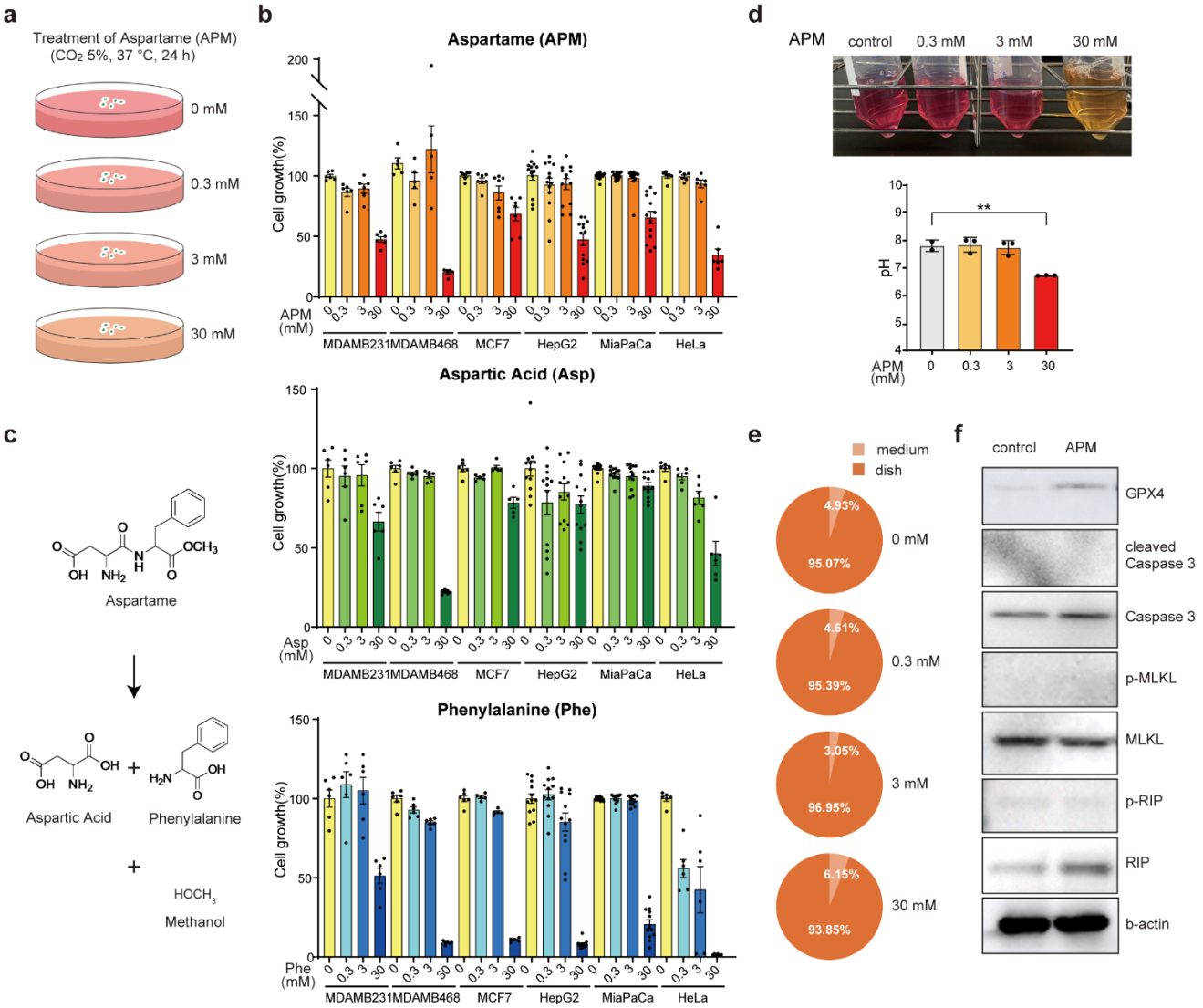

Figure 1. Effects of aspartame on cancer cell growth and cell death. **(a)** Cancer cells were cultured in DMEM (control) supplemented with 0.3 to 30 mM aspartame, aspartic acid, and phenylalanine; **(b)** Cell proliferation of Breast cancer, MDAMB231, MDAMB468, MCF7; Hepatic cancer, HepG2, Pancreatic cancer; MiaPaCa, Cervical cancer; HeLa and Colorectal cancer HCT116 cells cultured in DMEM supplemented with 0.3 to 30 mM aspartame, aspartic acid, or phenylalanine, measured at 72 h relative to 0 h. Data are presented as mean ± SEM. Not significant (ns), ****P < 0.0001 (one-way ANOVA with Tukey's test); **(c)** Aspartame is hydrolyzed into aspartic acid, phenylalanine, and methanol; **(d)** Aspartame increases the acidity of the medium. Supplementation with 0.3 to 30 mM aspartame gradually decreased the pH of the culture medium; **(e)** Proportion of floating cells in HCT116 cultures supplementation with Aspartame. Cells were counted after medium replacement for 24 h to determine the number of adherent (ad) and floating (fl) cells. The percentage of floating cells are shown below each pie chart; **(f)** Immunoblot analysis of cell death signaling (GPX4 for ferroptosis, cleaved caspase 3, caspase 3 for apoptosis, p-MLKL, MLKL, p-RIP, RIP for necroptosis, Actin for internal control) in HCT116 cells cultured in Control, Aspartame medium for 24 h.

3.2. Aspartame induces a conserved transcriptional program of xenobiotic metabolism and metallothionein suppression

To investigate the transcriptional responses induced by aspartame, RNA-seq was performed in HCT116 and HepG2 cells treated with 30 mM aspartame for 24 h, and DEGs between aspartame-treated and control cells were visualized using volcano plots (Figure 2a). To identify biological pathways altered by aspartame treatment, Reactome pathway enrichment analysis was performed separately for upregulated and downregulated genes in each cell line (Figure 2b). In both HCT116 and HepG2 cells, upregulated genes were enriched in pathways associated with xenobiotic metabolism and Phase I functionalization of compounds, suggesting activation of detoxification-related transcriptional programs, whereas downregulated genes were enriched in pathways related to metallothionein-mediated metal binding and the response to metal ions, indicating suppression of metal ion homeostasis and metal-responsive gene networks. To determine whether common transcriptional responses were induced across different cancer cell types, overlaps between DEGs identified in HCT116 and HepG2 cells were examined (Figure 2c). Among the commonly upregulated genes, CYP24A1 and DEPP autophagy regulator 1 (DEPP1) were identified as representative shared targets, whereas several metallothionein family genes and phosphatidylinositol glycan anchor biosynthesis class W (PIGW) were commonly downregulated in both cell lines. The expression patterns of these shared DEGs were further visualized using a heatmap (Figure 2d), demonstrating consistent regulation in both cell lines following aspartame treatment. Pathway enrichment analysis of the common DEGs revealed results similar to those observed in the individual cell lines (Figure 2e): commonly upregulated genes were enriched in pathways related to xenobiotic metabolism, Phase I functionalization, and cytochrome P450–associated processes, whereas commonly downregulated genes were strongly associated with metallothionein-mediated metal binding and cellular responses to metal ions. These findings indicate that aspartame induces a shared transcriptional signature, overlapping between the two cell lines, characterized by activation of detoxification-related pathways and suppression of metallothionein-dependent metal homeostasis across distinct cancer cell types.

To validate the RNA-seq findings, qPCR analysis was performed using representative genes that were commonly altered in both HCT116 and HepG2 cells (Figure 2f). CYP24A1 was selected as a representative upregulated gene, whereas MT1F was selected as a representative downregulated gene. Consistent with the RNA-seq results, CYP24A1 expression was significantly increased following aspartame treatment in both cell lines, whereas MT1F expression was markedly decreased in aspartame-treated cells compared with the corresponding controls. These results confirm the reliability of the RNA-seq analysis and demonstrate that aspartame induces reproducible transcriptional changes across multiple cancer cell types. RNA-seq data showed enrichment of xenobiotic metabolism pathways together with suppression of proliferation-associated pathways (E2 promoter-binding factor (E2F), MYC proto-oncogene, basic helix-loop-helix transcription factor (MYC), and mechanistic target of rapamycin complex 1 (mTORC1)). (Figure S1a). Although pentose phosphate pathway (PPP)-related genes were maintained or slightly increased (approximately 1.5-fold), canonical nuclear factor erythroid 2-related factor 2 (Nrf2) target genes were not consistently induced across cell lines (Figure S1b,c).

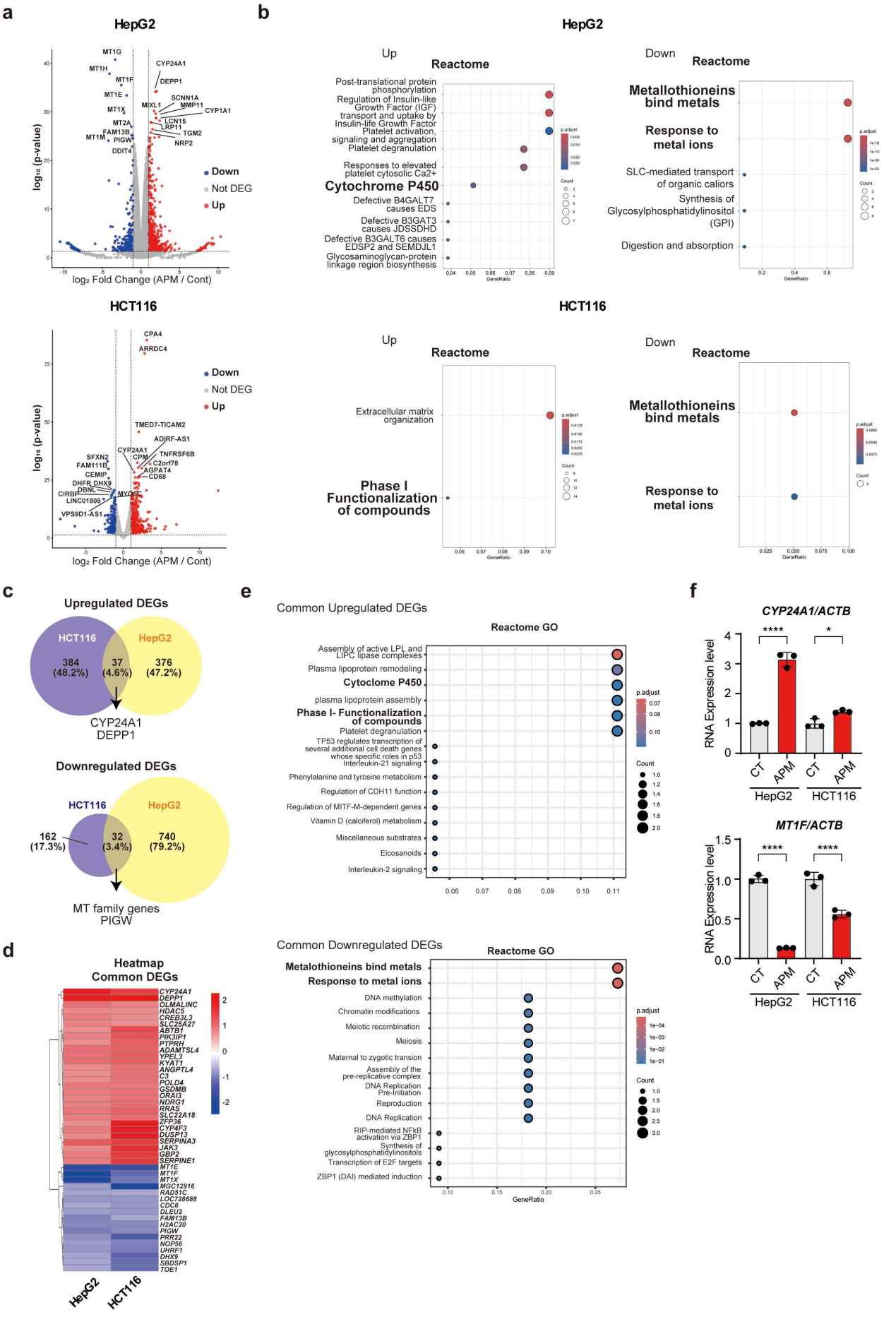
a
HepG2
log₁₀ (p-value)
log₂ Fold Change (APM / Cont)
Down
Not DEG
Up
MT1G
MT1H
MT1F
MT1E
MT1X
MT2A
MT1M
FAM13B
PIGW
DDIT4
CYP24A1
DEPP1
SCNN1A
MXL1
MMP11
CYP1A1
LCN15
LRP11
TGM2
NRP2
HCT116
CPA4
ARRDC4
TMED7-TICAM2
ADIRF-AS1
CYP24A1
CPM
TNFRSF6B
SFXN2
FAM111B
C2orf78
CEMIP
AGPAT4
CD68
DHFR_DHX9
DBNL
CIRBP
MYO9B
LINC01806
VPS9D1-AS1
b
HepG2
Up
Reactome
Post-translational protein phosphorylation
Regulation of Insulin-like Growth Factor (IGF) transport and uptake by Insulin-life Growth Factor
Platelet activation, signaling and aggregation
Platelet degranulation
Responses to elevated platelet cytosolic Ca2+
Cytochrome P450
Defective B4GALT7 causes EDS
Defective B3GAT3 causes JDSSDHD
Defective B3GALT6 causes EDSP2 and SEMDJL1
Glycosaminoglycan-protein linkage region biosynthesis
Down
Reactome
Metallothioneins bind metals
Response to metal ions
SLC-mediated transport of organic caliors
Synthesis of Glycosylphosphatidylinositol (GPI)
Digestion and absorption
HCT116
Up
Reactome
Extracellular matrix organization
Phase I Functionalization of compounds
Down
Reactome
Metallothioneins bind metals
Response to metal ions
c
Upregulated DEGs
HCT116
HepG2
384 (48.2%)
37 (4.6%)
376 (47.2%)
CYP24A1
DEPP1
Downregulated DEGs
HCT116
HepG2
162 (17.3%)
32 (3.4%)
740 (79.2%)
MT family genes
PIGW
d
Heatmap
Common DEGs
CYP24A1
DEPP1
OLMALINC
HDAC5
CREB3L3
SLC25A27
ABTB1
PIK3IP1
PTPRH
ADAMTSL4
YPEL3
KYAT1
ANGPTL4
C3
POLD4
GSDMB
ORAI3
NDRG1
RRAS
SLC22A18
ZFP36
CYP4F3
DUSP13
SERPINA3
JAK3
GBP2
SERPINE1
MT1E
MT1F
MT1X
MGC12916
RAD51C
LOC728688
CDC6
DLEU2
FAM13B
H2AC20
PIGW
PRR22
NOP56
UHRF1
DHX9
SBDSP1
TOE1
HepG2
HCT116
e
Common Upregulated DEGs
Reactome GO
Assembly of active LPL and LIPC lipase complexes
Plasma lipoprotein remodeling
Cytoclome P450
plasma lipoprotein assembly
Phase I- Functionalization of compounds
Platelet degranulation
TP53 regulates transcription of several additional cell death genes whose specific roles in p53
Interleukin-21 signaling
Phenylalanine and tyrosine metabolism
Regulation of CDH11 function
Regulation of MITF-M-dependent genes
Vitamin D (calciferol) metabolism
Miscellaneous substrates
Eicosanoids
Interleukin-2 signaling
p.adjust
Count
GeneRatio
Common Downregulated DEGs
Reactome GO
Metalothioneins bind metals
Response to metal ions
DNA methylation
Chromatin modifications
Meiotic recombination
Meiosis
Maternal to zygotic transion
Assembly of the pre-replicative complex
DNA Replication Pre-Initiation
Reproduction
DNA Replication
RIP-mediated NFkB activation via ZBP1
Synthesis of glycosylphosphatidylinositols
Transcription of E2F targets
ZBP1 (DAI) mediated induction
p.adjust
Count
GeneRatio
f
CYP24A1/ACTB
RNA Expression level
****
*
CT
APM
HepG2
HCT116
MT1F/ACTB
RNA Expression level
****
****
CT
APM
HepG2
HCT116

Figure 2. Transcriptional responses to aspartame in HCT116 and HepG2 cells. **(a)** Volcano plot showing DEGs in response to Aspartame in HCT116 and HepG2 cells. Upregulated genes (log2FC > 1, FDR < 0.05) are shown in red, downregulated genes (log2FC < −1, FDR < 0.05) in blue, and non-significant genes (|log2FC| ≤ 1) in black; **(b)** Pathway enrichment analysis of up/downregulated genes (log2FC < −1, p < 0.05) in response to Aspartame in HCT116 and HepG2 cells; **(c)** Venn diagram showing common genes upregulated (upper panel) and downregulated (lower panel) in cells exposed to Aspartame for 24 h, compared with control cells; **(d)** Heatmap of common genes upregulated and downregulated in cells exposed to Aspartame for 24 h, compared with control cells; **(e)** Pathway enrichment analysis of commonly up/downregulated genes (log2FC < −1, p < 0.05) in response to Aspartame in HCT116 and HepG2 cells; **(f)** mRNA expression levels of the commonly up/down-regulated genes in HCT116 and HepG2 cells in response to Aspartame. Data are presented as means ± SEM of n = 3 biological replicates. Statistical analysis was performed by one-way ANOVA. ∗p < 0.05, ∗∗∗∗p < 0.001.

3.3. Aspartame alters central carbon metabolism while suppressing biosynthetic and proliferative pathways

To investigate metabolic alterations induced by aspartame, metabolomic analyses were performed in HepG2 and HCT116 cells following treatment with 30 mM aspartame for 24 h, and differentially abundant metabolites between aspartame-treated and control cells were visualized using volcano plots (Figure 3a). Several metabolites were significantly altered in both cell lines: in HepG2 cells, increased levels of metabolites including fructose-6-phosphate, glucose-6-phosphate, citrate, and isocitrate were observed, while HCT116 cells exhibited increased levels of metabolites such as glutathione, creatinine, betaine aldehyde, and amino acid–related metabolites, whereas several sulfur amino acid metabolites were decreased, suggesting that aspartame induces broad metabolic remodeling across different cancer cell types. To further characterize the metabolic pathways upregulated by aspartame, pathway enrichment analysis was performed using the significantly increased metabolites in both cell lines (Figure 3b). The most prominently enriched pathways were related to central carbon metabolism, including glycolysis and gluconeogenesis. Pathways associated with metabolic reprogramming in cancer and the Warburg effect were also significantly enriched. Together, these findings suggest alterations in metabolites associated with glycolysis and glucose metabolism [19]. In addition, multiple pathways related to the PPP were significantly enriched, including pentose phosphate metabolism and the pentose phosphate cycle, as well as enzyme deficiency–associated pathways such as glucose-6-phosphate dehydrogenase and transaldolase deficiencies, consistent with alterations in metabolites linked to reduced nicotinamide adenine dinucleotide phosphate (NADPH)-generating and ribose-producing pathways [20]. Furthermore, pathways related to gluconeogenesis and glycogen metabolism, including glycogen storage disease-associated pathways, were enriched. Thiamine metabolism and glucagon signaling pathways were also enriched. Together, these findings are consistent with alterations in metabolites associated with glucose homeostasis and carbohydrate metabolism. Collectively, these findings demonstrate that aspartame treatment induces a marked reprogramming of central carbon metabolism characterized by alterations in glycolytic- and PPP-associated metabolites, together with altered regulation of glucose storage and production pathways, suggesting a shift in cellular energy and metabolic state.

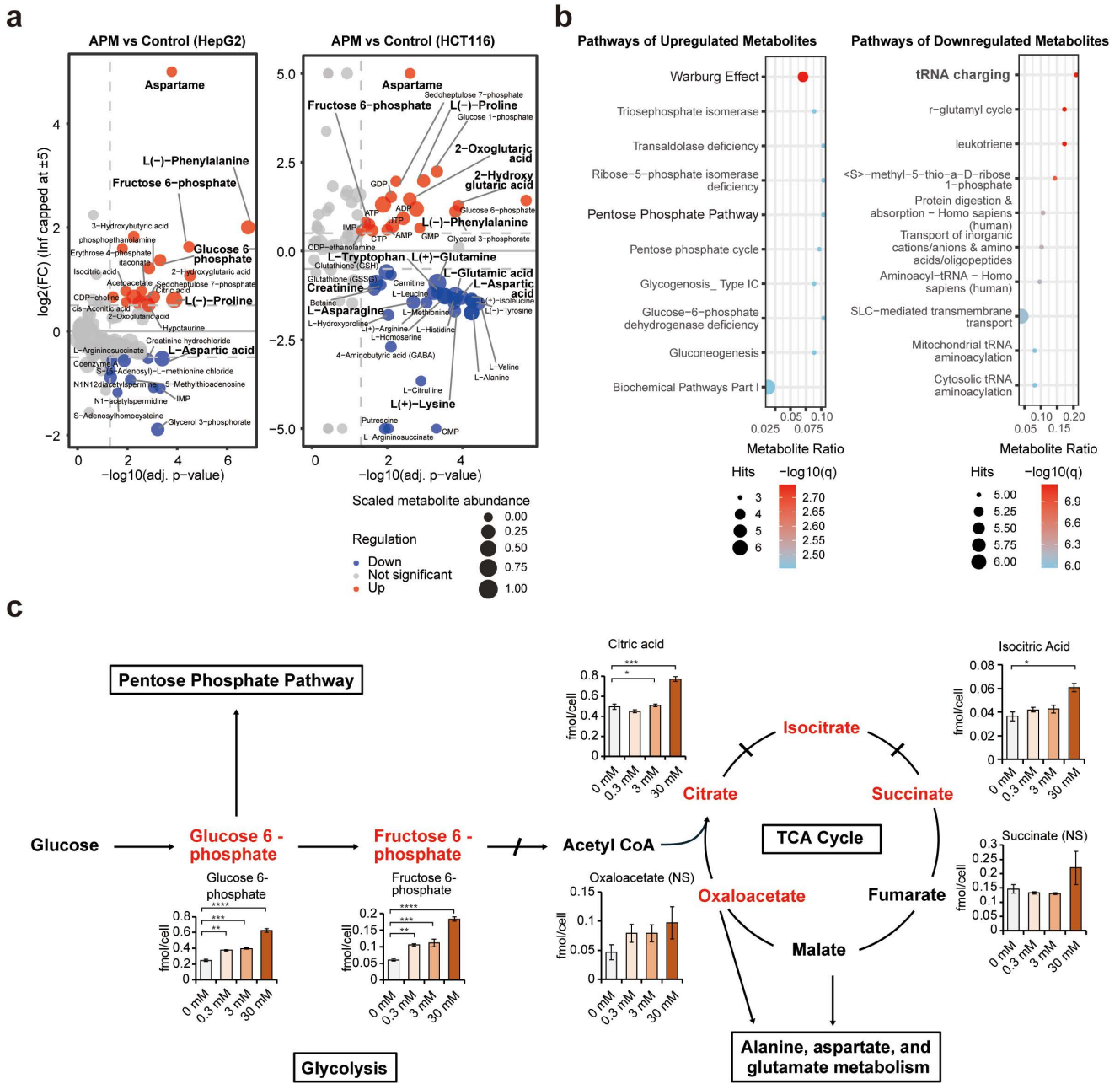

Figure 3. Metabolomic profiling of aspartame-treated cancer cells. **(a)** Volcano plots from capillary electrophoresis–mass spectrometry (CE-MS) metabolomics comparing metabolite abundance aspartame *vs.* Control. Each point represents a metabolite, with color indicating direction of change (red: increased in Aspartame; blue: decreased in Aspartame) and size reflecting relative mean abundance. Dashed lines indicate significance and fold-change thresholds; **(b)** Pathway enrichment analysis of aspartame-responsive metabolites. The left panel shows pathways enriched among aspartame-upregulated metabolites, and the right panel shows pathways enriched among aspartame-downregulated metabolites. Color indicates FDR (−log10 q value), and circle size represents the number of metabolites contributing to each pathway; **(c)** Schematic of the glycolysis and TCA cycle, indicating aspartame-responsive increases in glycolytic and TCA cycle metabolites. Intracellular metabolite levels (fmol/cell) of aspartame-responsive metabolites in HepG2. Data are presented as mean ± SEM. ns, *P < 0.05, **P < 0.01, ***P < 0.001, ****P < 0.0001 (one-way ANOVA with Tukey's test).

In contrast, downregulated pathways revealed a distinct metabolic signature associated with cellular biosynthetic and proliferative activity. Notably, pathways linked to nucleotide analog drug action, including mercaptopurine, thioguanine, and azathioprine metabolism (Small Molecule Pathway Database (SMPDB)), were significantly enriched, suggesting alterations in purine-associated metabolic networks, while Reactome analysis further indicated suppression of fundamental cellular processes, including cell cycle regulation (Cell Cycle, Mitotic), deoxyribonucleic acid (DNA) repair, and DNA double-strand break response. In addition, pathways related to ribosomal RNA (rRNA) processing, rRNA modification, and positive epigenetic regulation of rRNA expression were markedly downregulated, indicating suppression of ribosome biogenesis and translational capacity. Collectively, these results suggest that aspartame induces a metabolic state characterized by enhanced amino acid and carbohydrate-related metabolic activity while concurrently suppressing pathways associated with DNA replication, repair, and protein synthesis, indicating a reduction in proliferative biosynthetic programs accompanied by metabolic rewiring. Because pathway analysis suggested alterations in carbohydrate and amino acid metabolism, we next examined individual metabolites associated with glycolysis and the tricarboxylic acid (TCA) cycle (Figure 3c). Among glycolytic intermediates, glucose-6-phosphate and fructose-6-phosphate were increased following aspartame treatment in a concentration-dependent manner, and several TCA cycle intermediates, including citrate and isocitrate, were elevated, whereas oxaloacetate and succinate showed no statistically significant changes. These results indicate that aspartame alters selected metabolites within central carbon metabolism rather than uniformly activating the entire TCA cycle; the accumulation of citrate and isocitrate, together with increased glycolytic intermediates, suggests that aspartame alters the abundance of selected metabolites within central carbon metabolism; however, metabolite profiling alone cannot distinguish altered pathway flux from changes in metabolite pool size. Using pH- and osmolality-adjusted medium, metabolomic analysis showed that the number of upregulated pathways was decreased after adjustment, suggesting that the acidic pH and osmotic pressure account for part of the observed response (Figure S2a,b). However, major downregulated pathways, including amino acid metabolism, transfer RNA (tRNA) charging, aminoacyl-tRNA biosynthesis, and related metabolic programs, remained largely preserved (Figure S2c). Together, these findings suggest that medium acidification and osmotic stress contribute to, but do not fully account for, the observed metabolic remodeling.

3.4. Aspartame promotes tumor growth and alters tumor metabolism in vivo

To further evaluate the tumor-promoting potential of aspartame *in vivo*, a xenograft mouse model was established using HCT116 cells. Mice were subcutaneously injected with 1×10^7 cells per mouse, and tumor growth was monitored from day 6 to day 14 after implantation (approximately 8 days of aspartame administration). During the experimental period, the control group was provided with regular drinking water, whereas the aspartame-treated group received drinking water containing 30 mM aspartame (Figure 4a). As shown in Figure 4b, tumors in the aspartame-treated group exhibited a greater growth rate than those in the control group throughout the observation period, and by the end of the experiment tumor volume was significantly increased in the aspartame-treated group, indicating that aspartame intake promoted HCT116 tumor growth *in vivo*. In contrast, body weight did not differ significantly between the two groups (Figure 4c), and serum ALT, AST, TG, and cholesterol levels were comparable between control and aspartame-treated mice (Figure 4d), suggesting that the observed increase in tumor growth was not accompanied by overt systemic toxicity or liver dysfunction.

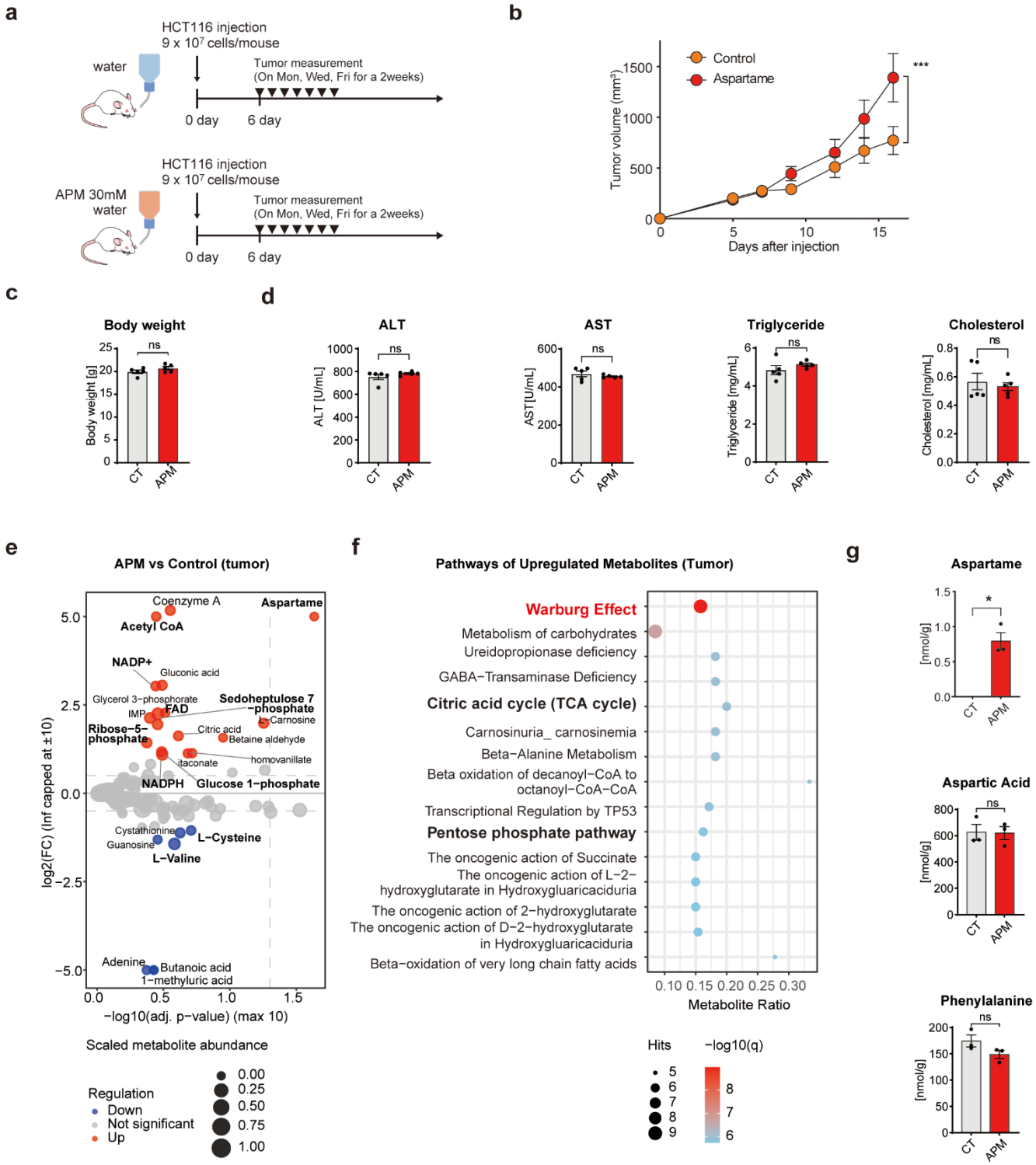

Figure 4. Effects of aspartame on tumor growth and tumor metabolism *in vivo*. **(a)** *In vivo* experiment scheme. Tumor cells (1 × 107 HCT116 cells suspended in 100 µL of PBS) were subcutaneously injected into severe combined immunodeficient (SCID) mice. Mice were treated with vehicle or Aspartame (30 mM, ad libitum in drinking water), starting from day 6 post-implantation; **(b)** Tumor growth curves of HCT116 tumors described in **(a)**. Tumor growth was monitored every 2 days (n = 5 mice per group). Tumor samples were collected for further analyses on day 14. Data are presented as means ± SEM of n = 5 biological replicates. Statistical analysis was performed by two-way repeated-measures ANOVA (mixed-effects model). ∗p < 0.05, ∗∗∗∗p < 0.001; ns; **(c)** Body weight of the mice treated with Aspartame. Body weight was measured on day 14 (n = 5).

Data are presented as means ± SEM of n = 5 biological replicates. Statistical analysis was performed by two-way ANOVA. ∗p < 0.05, ∗∗∗∗p < 0.001; ns; **(d)** ALT, AST, TG, and cholesterol in the plasma of aspartame *vs.* control mice were measured; **(e)** Volcano plots from CE-MS metabolomics comparing metabolite abundance *in vivo* tumors of aspartame *vs.* Control. Each point represents a metabolite, with color indicating direction of change (red: increased in Aspartame; blue: decreased in Aspartame) and size reflecting relative mean abundance. Dashed lines indicate significance and fold-change thresholds; **(f)** Pathway enrichment analysis of aspartame-responsive metabolites *in vivo*. The panel shows pathways enriched among aspartame-upregulated metabolites. Color indicates FDR, and circle size represents the number of metabolites contributing to each pathway; **(g)** Quantification of aspartame and its major hydrolysis products (phenylalanine and aspartic acid) in xenograft tumors from control and aspartame-treated mice. Metabolite levels are expressed as nmol/g tissue. Data are presented as mean ± SEM. Statistical significance was determined by Student's t-test. ns; *P < 0.05.

To investigate metabolic alterations associated with aspartame-induced tumor growth, metabolomic profiling was performed on excised tumor tissues, which revealed substantial metabolic changes in tumors from aspartame-treated mice (Figure 4e). Pathway enrichment analysis showed that upregulated metabolites were significantly associated with pathways involved in central carbon metabolism, including the Warburg effect, carbohydrate metabolism, the PPP, and the TCA cycle (Figure 4f), whereas downregulated metabolites were enriched in pathways related to glucose homeostasis, tRNA charging, the γ-glutamyl cycle, amino acid metabolism, and cysteine biosynthesis. Detailed pathway analysis of downregulated metabolites is provided in Figure S3, in which glucose homeostasis emerged as the most significantly enriched pathway. Representative metabolites associated with these pathways are shown in Figure S4. Although individual metabolite responses varied, their overall direction was consistent with the pathway enrichment analysis. Importantly, intact aspartame was detected within tumors from treated mice, whereas phenylalanine and aspartic acid levels were not significantly different between groups (Figure 4g). Furthermore, our RNA-seq re-analysis did not support activation of mTORC1 signaling (Figure S1a). These findings argue against a simple explanation based on accumulation of the major hydrolysis products and support the interpretation that the observed metabolic alterations cannot be readily attributed to phenylalanine or aspartic acid alone. Together, the pathway-level analyses support broad metabolic remodeling in tumors from aspartame-treated mice.

4. Conclusion

In this study, we comprehensively investigated the effects of aspartame on cancer cells using integrated transcriptomic and metabolomic analyses. Although aspartame produced only modest effects on short-term cell proliferation and did not induce substantial apoptotic or necroptotic cell death, it elicited pronounced transcriptional and metabolic alterations. Importantly, continuous (day 6–14, approximately 8 days) exposure to aspartame promoted tumor growth in a colorectal cancer xenograft model, suggesting that its biological effects may become more evident at the level of tumor metabolism and tumor progression rather than through direct cytotoxicity.

RNA-seq analysis revealed a conserved transcriptional response across HCT116 and HepG2 cells characterized by induction of xenobiotic metabolism–related pathways and suppression of metallothionein-associated gene networks. The upregulation of detoxification-related genes may reflect

a cellular adaptation to the presence of aspartame or its metabolites [21]. Re-analysis of the RNA-seq dataset further showed suppression of E2F, MYC, and mTORC1-associated programs, whereas canonical Nrf2 target genes were not consistently induced, suggesting that the observed transcriptional response is more consistent with a stress/detoxification program than with a dedicated pro-growth metabolic state. Conversely, downregulation of metallothionein family genes suggests altered metal ion homeostasis, which could influence multiple cellular processes including oxidative stress responses and metabolic regulation [22,23]. Although the functional significance of these transcriptional changes remains to be determined, they indicate that aspartame exposure is sufficient to trigger broad cellular adaptation programs.

The most prominent finding of this study was the extensive metabolic remodeling associated with high-concentration aspartame exposure. Metabolomic analyses consistently demonstrated enrichment of pathways associated with glycolysis, the PPP, central carbon metabolism, and the Warburg effect. Increased levels of glucose-6-phosphate, fructose-6-phosphate, citrate, isocitrate, acetyl-coenzyme A (acetyl-CoA), and coenzyme A (CoA) were also observed. These observations suggest that aspartame exposure is associated with metabolic states that share features with central carbon metabolic programs observed in cancer cells [14,19,20]. Interestingly, however, not all metabolic changes were consistent with a simple increase in proliferative activity: pathways related to cell cycle progression, DNA repair, and ribosome biogenesis were downregulated in the *in vitro* analyses, and several amino acid–related pathways, including tRNA charging, amino acid metabolism, and cysteine biosynthesis, were reduced in tumors from aspartame-treated mice. These findings suggest that aspartame does not uniformly stimulate all anabolic processes but rather induces selective metabolic rewiring; one possible explanation is that alterations in central carbon metabolism may be accompanied by increased consumption of specific amino acids required to sustain tumor growth, resulting in reduced steady-state levels of metabolites such as valine, isoleucine, and methionine within tumor tissues [24–27].

Beyond their bioenergetic and biosynthetic roles, several of the intermediates that accumulated following aspartame exposure are closely linked to the regulation of gene expression [28–31]. Citrate and isocitrate feed into the production of α-ketoglutarate and related TCA cycle metabolites, whose relative abundance governs the activity of α-ketoglutarate–dependent dioxygenases, including ten-eleven translocation (TET) DNA demethylases and Jumonji-C histone demethylases [30,32–34]. Imbalances among these metabolites can therefore reshape DNA and histone methylation, and the concurrent suppression of cell cycle, DNA repair, and ribosome biogenesis pathways observed here is consistent with such metabolic–epigenetic crosstalk. Because epigenetic alterations are recognized as a key characteristic of carcinogens yet remain among the least explored aspects of aspartame's biology, our findings raise the possibility that aspartame-induced metabolic remodeling may contribute to a permissive epigenetic state, a hypothesis that warrants direct testing in future studies [35].

The *in vivo* metabolomic findings further strengthen the link between aspartame exposure and metabolic reprogramming. Tumors from aspartame-treated mice exhibited increased levels of acetyl-CoA, citrate, and CoA together with enrichment of pathways related to the Warburg effect and the TCA cycle. Importantly, these findings do not support a simple explanation based on accumulation of the major hydrolysis products. Rather, they suggest that the tumor-associated metabolic alterations observed in the present study reflect a broader response to high-concentration aspartame exposure. These changes were accompanied by significantly accelerated tumor growth despite the absence of detectable changes in body weight, liver enzymes, TG, or cholesterol levels. Therefore, the tumor-promoting effects observed in

this study are unlikely to be explained by overt systemic toxicity and instead appear to be associated with local metabolic alterations within the tumor microenvironment.

In conclusion, our integrated transcriptomic and metabolomic analyses demonstrate that aspartame induces substantial metabolic and transcriptional reprogramming in cancer cells despite exerting only limited effects on short-term cell proliferation or cell death. The observed metabolic remodeling together with accelerated tumor growth *in vivo* suggests that aspartame may influence cancer progression primarily through metabolic adaptation rather than direct cytotoxic effects. These findings further raise the possibility that metabolic remodeling induced by aspartame contributes to epigenetic regulation, providing a potential mechanistic link between metabolic alterations and tumor-promoting activity.

Several limitations of this study should be acknowledged. First, the concentration of aspartame used *in vitro* was substantially higher than typical human exposure levels and therefore may not directly reflect physiological conditions, so caution is required when extrapolating these findings to dietary aspartame consumption in humans. The estimated human equivalent dose (~125 mg/kg/day) exceeds the current acceptable daily intake (40 mg/kg/day), indicating that the present study represents a high-exposure experimental condition. Rather than demonstrating a direct carcinogenic effect of aspartame under normal exposure conditions, our findings indicate that excessive aspartame exposure has the potential to alter cancer cell metabolism in a manner that may favor tumor progression. Nevertheless, local concentrations of dietary compounds can differ substantially from systemic circulating levels; following ingestion, aspartame and its metabolites may transiently accumulate in specific tissues or microenvironments before being fully metabolized and cleared, so the possibility that localized metabolic effects contribute to biological responses cannot be completely excluded. Because concentrated aspartame exposure inherently altered the extracellular environment, including medium pH and osmolality, these factors should be regarded as part of the overall cellular response observed under the present experimental conditions. Control experiments performed under pH- and osmolality-adjusted conditions suggested that environmental changes contribute to a portion of the metabolic response, although they did not fully account for the observed metabolomic alterations. Notably, several downregulated pathways, including amino acid metabolism and tRNA charging, remained preserved after pH and osmolality adjustment, suggesting that environmental changes contribute to, but do not fully account for, the observed metabolic remodeling [36,37]. Metabolomic analyses provide information regarding metabolite abundance but do not directly measure metabolic flux. Future studies incorporating stable isotope tracing, glucose uptake, lactate production, and flux analyses will therefore be required to determine whether aspartame directly contributes carbon to central metabolic pathways or indirectly alters metabolic network activity [38]. Further studies using physiologically relevant exposure conditions and multiple tumor models will also be necessary to clarify the potential relationship between long-term aspartame consumption and cancer progression.

Data availability statement

The RNA-seq data generated in this study have been deposited in the DNA Data Bank of Japan (DDBJ) and are publicly available under BioProject accession number PRJDB43016. The corresponding DDBJ Sequence Read Archive (DRA) accession numbers are DRX1256304–DRX1256321 (experiments) and DRR1291657–DRR1291674 (runs). Supplementary material accompanying this article includes Figures S1–S4, which provide additional transcriptomic and metabolomic analyses. Other data supporting the findings of this study are available from the corresponding author upon reasonable request.

Declaration of generative and AI-assisted technologies

During the preparation of this manuscript, the authors used ChatGPT only for language polishing and copy editing. The tool was not used to generate or develop scientific content. The authors reviewed and verified all AI-assisted edits and take full responsibility for the integrity, originality, and accuracy of the manuscript.

Acknowledgments

We thank the members of the Division of Nutriomics and Oncology, Laboratory for Systems Biology and Medicine, Genome Science and Medicine, the RCAST, University of Tokyo for helpful discussions and support. This work was supported by Grant-in-Aid for Scientific Research (B) (T.O.) and (C) (24K10279, K.Y.), Grant-in-Aid for Transformative Research Areas (A) (25H01339 and 25A304 to T.O.) and (B) (23H03861 to C.I.-Y. and K.Y), Grant-in-Aid for Scientific Research on Innovative Areas (20H04834 to T.O.) and Grants-in-Aid for Challenging Exploratory Research (19K22553, 21K19399, 23K18234, and 25K22572 to T.O.). We also acknowledge support from Japan Society for the Promotion of Science (JSPS) KAKENHI grant Advanced Animal Model Support (AdAMS; 22H04922) from the Ministry of Education, Culture, Sports, Science and Technology of Japan, the SGH Foundation (T.O.), the Canon Foundation (T.O.), the Takeda Foundation (T.O.), and the Princess Takamatsu Cancer Foundation (T.O.). This research was also supported by Japan Agency for Medical Research and Development (AMED) (T.O.). This work was also supported by Japan Science and Technology Agency (JST) Fusion Oriented Research for disruptive Science and Technology (FOREST) Program, grant number JPMJFR2306 (T.O.). This study was supported partly by Institute of Science, Tokyo, an Extramural Collaborative Research grant, the Cancer Research Institute, Kanazawa University, and a grant from the Joint Research Program of Institute for Genetic Medicine, Hokkaido University.

Authors' contribution

Conceptualization, M.S. and T.O.; validation, M.S., H.I., A.F., B.X., C.I., Y.Y. and Z.Z.; formal analysis, H.I., A.F., B.X., C.I., R.A., Y.Y.; investigation, M.S., H.I., A.F., T.O.; resources, K.Y.; data curation, M.S., C.I., K.Y.; writing—original draft preparation, H.I., A.S., B.X., C.B., T.O.; writing—review and editing, A.S., B.X, C.B., T.O.; visualization, R.A.; supervision, T.O.; project administration, R.T., T.O.; funding acquisition, T.O.; All authors have read and agreed to the published version of the manuscript.

Conflicts of interest

Tsuyoshi Osawa holds the position of Editorial Board Member for *Advanced Cancer Research* and has not peer reviewed or made any editorial decisions for this paper. The authors disclose no knowledge of any potential conflicts of interest.

Ethical statement

All animal experiments were approved by the Research Center for Advanced Science and Technology (RCAST), The University of Tokyo (approval date: May 31, 2023; approval number: RAC230006).

References

[1] Huang Y, Chen Z, Chen B, Li J, Yuan X, *et al.* Dietary sugar consumption and health: umbrella review. *BMJ* 2023, 381:e071609.

[2] Meng Y, Li S, Khan J, Dai Z, Li C, *et al.* Sugar- and artificially sweetened beverages consumption linked to type 2 diabetes, cardiovascular diseases, and all-cause mortality: a systematic review and dose-response meta-analysis of prospective cohort studies. *Nutrients* 2021, 13(8):2636.

[3] Llaha F, Gil-Lespinard M, Unal P, Villasante I de, Castañeda J, *et al.* Consumption of sweet beverages and cancer risk. A systematic review and meta-analysis of observational studies. *Nutrients* 2021, 13(2):516.

[4] Zhang S, Xiao Y, Cheng Y, Ma Y, Liu J, *et al.* Associations of sugar intake, high-sugar dietary pattern, and the risk of dementia: a prospective cohort study of 210,832 participants. *BMC Med.* 2024, 22(1):298.

[5] Magnuson BA, Burdock GA, Doull J, Kroes RM, Marsh GM, *et al.* Aspartame: a safety evaluation based on current use levels, regulations, and toxicological and epidemiological studies. *Crit. Rev. Toxicol.* 2007, 37(8):629–727.

[6] Debras C, Chazelas E, Srour B, Druesne-Pecollo N, Esseddik Y, *et al.* Artificial sweeteners and cancer risk: results from the NutriNet-Santé population-based cohort study. *PLoS Med.* 2022, 19(3):e1003950.

[7] U.S. Food and Drug Administration. Aspartame and Other Sweeteners in Food. 2025. Available: https://www.fda.gov/food/food-additives-petitions/aspartame-and-other-sweeteners-food (accessed on 29 June 2026).

[8] EFSA. Re-evaluation of salt of aspartame-acesulfame (E 962) as food additive. 2026. Available: https://efsa.onlinelibrary.wiley.com/doi/10.2903/j.efsa.2026.10259 (accessed on 29 June 2026).

[9] Magnuson BA, Carakostas MC, Moore NH, Poulos SP, Renwick AG. Biological fate of low-calorie sweeteners. *Nutr. Rev.* 2016, 74(11):670–689.

[10] Riboli E, Beland FA, Lachenmeier DW, Marques MM, Phillips DH, *et al.* Carcinogenicity of aspartame, methyleugenol, and isoeugenol. *Lancet Oncol.* 2023, 24(8):848–850.

[11] World Health Organization. Aspartame hazard and risk assessment results released. 2023. Available: https://www.who.int/news/item/14-07-2023-aspartame-hazard-and-risk-assessment-results-released (accessed on 29 June 2026).

[12] International Agency for Research on Cancer. *Aspartame, Methyleugenol, and Isoeugenol (IARC Monographs on the Identification of Carcinogenic Hazards to Humans, Volume 134)*. Lyon: IARC, 2024. pp. 1–542.

[13] Hanahan D. Hallmarks of cancer: new dimensions. *Cancer Discovery* 2022, 12(1):31–46.

[14] Pavlova NN, Thompson CB. The emerging hallmarks of cancer metabolism. *Cell Metab.* 2016, 23(1):27–47.

[15] DeBerardinis RJ, Chandel NS. Fundamentals of cancer metabolism. *Sci. Adv.* 2016, 2(5):e1600200.

[16] Auslander N, Yizhak K, Weinstock A, Budhu A, Tang W, *et al.* A joint analysis of transcriptomic and metabolomic data uncovers enhanced enzyme-metabolite coupling in breast cancer. *Sci. Rep.* 2016, 6:29662.
[17] Vichai V, Kirtikara K. Sulforhodamine B colorimetric assay for cytotoxicity screening. *Nat. Protoc.* 2006, 1(3):1112–1116.
[18] Gong Y, Fan Z, Luo G, Yang C, Huang Q, *et al.* The role of necroptosis in cancer biology and therapy. *Mol. Cancer* 2019, 18(1):100.
[19] Vander Heiden MG, Cantley LC, Thompson CB. Understanding the Warburg effect: the metabolic requirements of cell proliferation. *Science* 2009, 324(5930):1029–1033.
[20] Patra KC, Hay N. The pentose phosphate pathway and cancer. *Trends Biochem. Sci.* 2014, 39(8):347–354.
[21] Tamási V, Monostory K, Prough RA, Falus A. Role of xenobiotic metabolism in cancer: involvement of transcriptional and miRNA regulation of P450s. *Cell Mol. Life Sci*. 2011, 68(7):1131–1146.
[22] Si M, Lang J. The roles of metallothioneins in carcinogenesis. *J. Hematol. Oncol.* 2018, 11(1):107.
[23] Ruttkay-Nedecky B, Nejdl L, Gumulec J, Zitka O, Masarik M, *et al.* The role of metallothionein in oxidative stress. *Int. J. Mol. Sci.* 2013, 14(3):6044–6066.
[24] Sivanand S, Vander Heiden MG. Emerging roles for branched-chain amino acid metabolism in cancer. *Cancer Cell* 2020, 37(2):147–156.
[25] Sanderson SM, Gao X, Dai Z, Locasale JW. Methionine metabolism in health and cancer: a nexus of diet and precision medicine. *Nat. Rev. Cancer* 2019, 19(11):625–637.
[26] Lieu EL, Nguyen T, Rhyne S, Kim J. Amino acids in cancer. *Exp. Mol. Med.* 2020, 52(1):15–30.
[27] Vettore L, Westbrook RL, Tennant DA. New aspects of amino acid metabolism in cancer. *Br. J. Cancer* 2020, 122(2):150–156.
[28] Wellen KE, Hatzivassiliou G, Sachdeva UM, Bui TV, Cross JR, *et al.* ATP-citrate lyase links cellular metabolism to histone acetylation. *Science* 2009, 324(5930):1076–1080.
[29] Pietrocola F, Galluzzi L, Bravo-San Pedro JM, Madeo F, Kroemer G. Acetyl coenzyme A: a central metabolite and second messenger. *Cell Metab*. 2015, 21(6):805–821.
[30] Janke R, Dodson AE, Rine J. Metabolism and epigenetics. *Annu. Rev. Cell Dev. Biol*. 2015, 31:473–496.
[31] Martínez-Reyes I, Chandel NS. Mitochondrial TCA cycle metabolites control physiology and disease. *Nat. Commun.* 2020, 11(1):102.
[32] Xu W, Yang H, Liu Y, Yang Y, Wang P, *et al.* Oncometabolite 2-hydroxyglutarate is a competitive inhibitor of α-ketoglutarate-dependent dioxygenases. *Cancer Cell* 2011, 19(1):17–30.
[33] Xiao M, Yang H, Xu W, Ma S, Lin H, *et al.* Inhibition of α-KG-dependent histone and DNA demethylases by fumarate and succinate that are accumulated in mutations of FH and SDH tumor suppressors. *Genes Dev.* 2012, 26(12):1326–1338.
[34] Osawa T, Muramatsu M, Wang F, Tsuchida R, Kodama T, *et al.* Increased expression of histone demethylase JHDM1D under nutrient st arvation suppresses tumor growth via down-regulating angiogenesis. *Proc. Natl. Acad. Sci. U. S. A.* 2011, 108(51):20725–20729.
[35] Smith MT, Guyton KZ, Kleinstreuer N, Borrel A, Cardenas A, *et al.* The key characteristics of carcinogens: relationship to the hallmarks of cancer, relevant biomarkers, and assays to measure them. *Cancer Epidemiol. Biomark. Prev.* 2020, 29(10):1887–1903.

[36] Kondo A, Yamamoto S, Nakaki R, Shimamura T, Hamakubo T, *et al.* Extracellular acidic pH activates the sterol regulatory element-binding protein 2 to promote tumor progression. *Cell Rep.* 2017, 18(9):2228–2242.

[37] Hasegawa M, Xu B, Maeda K, Seki M, Cai F, *et al.* Tolerance to extracellular acidic pH facilitates tumor plasticity. *Cell Rep.* 2026, 45(4):117226.

[38] Reisz JA, D'Alessandro A. Measurement of metabolic fluxes using stable isotope tracers in whole animals and human patients. *Curr. Opin. Clin. Nutr. Metab. Care* 2017, 20(5):366–374.